Improvements of Biogenic Emission Estimation in China by Using WRF-CLM4-MEGAN Model

Lifei Yin[1], Zhenying Xu[1], Mingxu Liu[1], Tingting Xu[1,2], Tiantian Wang[1], Wenling Liao[1], Mengmeng Li[3], Xuhui Cai[1], Ling Kang[1], Hongsheng Zhang[4], Yu Song[1]

[1]State Key Joint Laboratory of Environmental Simulation and Pollution Control, Department of Environmental Science, Peking University, Beijing 100871, China.

[2]Environmental College, Chengdu University of Technology, Chengdu 610059, China.

[3]School of Atmospheric Sciences, Nanjing University, Nanjing 210000, China.

[4]Laboratory for Climate and Ocean-Atmosphere Studies, Department of Atmospheric and Oceanic Sciences, School of Physics, Peking University, Beijing 100871, China.

Corresponding author: Yu Song (songyu@pku.edu.cn)

Key Points:

- Regional biogenic emissions were estimated within an ecological framework base on plant-specific physiological parameters.
- Neglect of leaf-air temperature bias and shaded canopy resulted in a 23% decrease and a 102% increase in estimation, respectively.
- Simulated isoprene flux was generally within a factor of 2 of canopy-scale flux measurements, indicating the good performance of this method.

Abstract

Biogenic emission models are developed on the foundation of leaf physiological processes and driven by a set of physical and biological factors. To estimate emissions online, many studies used weather forecasting models coupled with simple biogenic emission algorithms, in which the canopy physiological parameters were neglected or oversimplified. In this study, the land surface scheme CLM4 (Community Land Model version 4) coupled in the advanced Weather Research and Forecasting model (WRF) was used to determine canopy physiological parameters. The MEGAN (Model of Emissions of Gases and Aerosols from Nature) algorithms embedded in CLM4 scheme used these parameters to estimate biogenic emissions. The emission estimated by using leaf temperature in our study were about 23% higher than that based on air temperature as in the previous methods. Compared with studies neglecting shaded canopy, the separate treatments of sunlit and shaded leaves in this study lowered the estimations by a factor of 2 through decreasing diffuse radiaton absorbed by sunlit canopy. Dynamic weather history was used in our study to replace the fixed values in the original MEGAN-CLM4 code. An emission inventory of isoprene and monoterpenes in China was established for the year 2018. The estimates were evaluated against field measurements. Generally, the coupled model produced a reasonable simulation in both emission budgets and spatiotemporal distribution of biogenic emissions.

Plain Language Summary

The gas emission rate of vegetation depends on physiological conditions such as leaf temperature, stomatal opening, and absorbed radiation. We estimated regional vegetation emissions based on plant physiological parameters, which were neglected or oversimplified in previous studies. Emission estimations based on leaf temperature in our study were 23% higher than estimations based on air temperature in previous studies. Neglecting the shaded canopy overestimated emissions by a factor of 2 compared with estimations in our study, which treated sunlit and shaded leaves separately. The effects of weather history on emission rates were considered in our study. Comparisons between simulated and measured emissions showed that this method was able to estimate vegetation emissions reasonably.

1 Introduction

Globally speaking, biogenic volatile organic compounds (BVOCs) emitted by terrestrial vegetation are estimated to be 500~1100 Tg C yr^{-1}, corresponding to about 90% of the emission total (Guenther et al., 1995; Henrot et al., 2017). Many BVOC species are actively involved in the atmospheric chemistry and have a substantial impact on tropospheric oxidation, aerosol concentration, and the global carbon cycle (Fehsenfeld et al., 1992). BVOCs are therefore a crucial component of the earth system and quantitative estimates of their emissions are required for further exploring their impacts on regional and global atmospheric chemistry.

Many biogenic emission models are developed with a strong foundation in the physiological processes of a leaf (Guenther et al., 1991; Niinemets et al., 1999). The Model of Emissions of Gases and Aerosols from Nature (MEGAN), a model estimates BVOC emission fluxes as basal emission rates modulated by emission activity factors, has been intensively used for regional and global BVOC emission estimations (Guenther et al., 2006; Guenther et al., 2012). Process-based models link BVOC production rate explicitly to leaf photosynthetic electron transport rate and election requirement for BVOC synthesis (Niinemets et al., 2002; Niinemets et al., 1999).

The MEGAN algorithms are incorporated into the terrestrial component of the earth climate system model, Community Land Model (CLM) for online estimation. In the coupling of MEGAN and CLM, physical and biological variables required by BVOC estimation are determined by comprehensive ecological and physiological processes in CLM at each time step (Lawrence et al., 2011; Levis et al., 2003). Process-based models are typically coupled within dynamic vegetation models that have a mechanistic model for leaf photosynthesis at their core (Arneth et al., 2007). These models require more computational time and resources, so it would be too time-consuming for regional emission estimation.

Instead, many studies use weather forecasting models coupled with a simplified version of MEGAN, the parameterized canopy emission activity (PCEEA) algorithm (Guenther et al., 2006; Sakulyanontvittaya et al., 2008). Due to lack of a detailed canopy model which calculates leaf temperature and leaf-level photosynthetic photon flux density (PPFD), the PCEEA algorithm uses air temperature and canopy above solar radiation instead. The leaf temperature is affected by air temperature, as well as other environmental and biological factors. Subin et al. (2011) indicates that the strong advection and boundary layer mixing during the day decouples the air temperature from the vegetation temperature to a great extent, making daytime surface energy budget the primary controlling factors of vegetation temperature changes. Furthermore, due to the different morphological and physiological properties, relationships between air temperature and leaf temperature, and between canopy above PPFD and leaf-level PPFD, vary significantly among tree species. Since the PCEEA algorithm was based on standard MEGAN canopy model simulation for warm broadleaf forests, using the same equations for representations of other plant types leads to unpredictable uncertainties. Therefore, reasonable plant-specific physiological variables are needed to improve the BVOC estimation in weather models.

CLM version 4 (CLM4) was coupled and released with the Weather Research and Forecasting model (WRF), a mesoscale numerical model designed to simulate regional weather and climate, as one of the land surface scheme options (Jin et al., 2010). Because MEGAN has been embedded within CLM as mentioned above, the coupling of WRF-CLM4-MEGAN allowed weather forecasting models to estimate regional BVOC emissions within an ecological framework. Besides improvements result from real-time plant physiological variables derived from CLM4, sub-grid vegetation compositions represented in CLM4 are also expected to provide a more reasonable estimation because of the significant variability in basal emission ability among tree species. However, few studies employed the coupled model to estimate regional BVOC emissions (Zhao et al., 2016).

Satellite data revealed a significant greening pattern in China from the year 2000 to 2017. Approximately 42% of the greening in China was associated with forest explanation to mitigate land degradation, air pollution, and climate change (Chen et al., 2019) (Chen et al., 2019). Accurate estimations are needed to investigate the trend in BVOC emissions with changes in land cover. In recent decades, many studies estimated national or regional BVOC emissions and reported a wide emission range of 4.1~23.4 Tg C yr^{-1} for isoprene and 1.8~5.6 Tg C yr^{-1} for monoterpenes on the national level (Fu and Liao, 2012; Klinger et al., 2002; Li et al., 2013; Liu et al., 2018; Tie et al., 2006; Wu et al., 2020). However, these estimates are either calculated offline or not fully based on plant physiological variables. In this study, we used the WRF-CLM4-MEGAN coupled model to improve BVOC emission estimations in China. Two primary classes of BVOCs, isoprene (C_5H_8) and monoterpenes ($C_{10}H_{16}$) (including α-pinene, β-pinene, 3-carene, t-β-ocimene, limonene, sabinene, and myrcene), were considered in this study.

2 Methods and Data

2.1 CLM4 land surface scheme and coupling with MEGAN

The CLM4 was coupled and released with WRF since version 3.5 as one of the land surface scheme options. CLM4 consists of components related to land biogeophysics, hydrological cycle, biogeochemistry, human dimensions, and ecosystem dynamics. CLM4 includes 5 layers for snow, 10 layers for soil, and 1 layer for vegetation and is accurate in describing soil and vegetation processes (Jin and Wen, 2012; Lawrence et al., 2011; Subin et al., 2011).

The MEGAN model uses mechanistic algorithms to account for the major known process controlling biogenic emissions. MEGAN estimates emissions (F_i, μg C m^{-2} ground area h^{-1}) of BVOC species *i* according to:

$$F_i = \gamma_i \times \sum \varepsilon_{i,j} \times \chi_j \tag{1}$$

where $\varepsilon_{i,j}$ (μg C m^{-2} h^{-1}) is the emission factor (EF) at standard conditions for PFT *j* with fraction coverage χ_j. PFT-specific EFs of isoprene were determined based on observations conducted in China and EF used in previous studies (as shown in Table S1). Due to lack of detailed monoterpene EFs reports, the EFs of main monoterpene species were determined by scaling default MEGAN EFs with the ratio of local isoprene EF to default value presented in Guenther et al. (2012)). The emission factors of each vegetation type used in this study were shown in Table S2.

The emission activity factor for each compound (γ_i) accounts for emission responses to solar radiation, leaf temperature, LAI, leaf age, and soil moisture. The effects of variations in CO_2 concentration were neglected in this study. Details of the algorithms could be found in Guenther et al. (2006) and Guenther et al. (2012).

The coupling of CLM4-MEGAN improves the BVOC estimations through reasonable driving factors and detailed sub-grid representation, as briefly described below. We refer the reader to the description of Oleson et al. (2010) for the details of computations.

1. Leaf temperature

Variations in leaf temperature are influenced by net radiation absorbed/emitted by the vegetation and sensible and latent heat fluxes from vegetation. The two-stream approximation is applied to vegetation when calculating solar radiation reflected and absorbed by the canopy. Leaf temperatures are determined by the canopy energy balance equations. Due to the dependence of heat fluxes on vegetation temperature, the Newton-Raphson iteration is used to solve for folia temperature and the vegetation fluxes simultaneously.

2. Sunlit and shaded fractions of the canopy

The canopy in CLM4 is treated as sunlit and shaded leaves. Leaf fractions of different plant types are determined according to the leaf and stem area index and the solar zenith angle at each time step. CLM4 assumed that sunlit leaves receive the absorbed direct beam radiation and the absorbed diffuse radiation apportioned by f_{sun} (the sunlit fraction of the canopy), and that shaded leaves receive the absorbed diffuse radiation apportioned by f_{sha} (the shaded fraction).

3. The medium-term weather history

Current MEGAN algorithms use average leaf temperature, solar radiation, and leaf fractions over the past time to account for the influence of medium-term (days to weeks) weather history. CLM4 contains an accumulation module used to calculate the average of user-specified variables over user-defined time intervals. However, the accumulation of past time leaf temperature and PPFD was commented out in the default CLM4 code. Instead, fixed values are assigned to those coefficients based on conditions during previous days. After activating this module, a decrease in average temperature and PPFD with increasing simulation time was found. That was because these two variables were not being accumulated but still being averaged over the total running time. We corrected the accumulation code so that the average leaf temperature, PPFD, and leaf fraction are calculated at each time step.

4. Sub-grid heterogeneity

In CLM4, the surface heterogeneity is represented using a sub-grid tile approach in which grid cells are composed of multiple land units (glacier, wetland, lake, urban and vegetated area), snow/soil columns and plant functional types (PFTs). Vegetated surfaces are comprised of up to 4 plant functional types (PFTs). An explicit canopy layer represents the PFTs with specific leaf and stem optical properties, root distribution parameters, aerodynamic parameters, and photosynthetic parameters. The detailed representations of sub-grid improve the accuracy of land surface parameterizations and reduce the uncertainty from plant distribution in BVOC estimation (Schultz et al., 2016; Zhao et al., 2016).

2.2 Land surface datasets

In this study, MODIS datasets of land cover (MCD12Q1) for the year 2016 and water mask (MOD44W) for the year 2015, both with a resolution of 500 m, were used to replace the outdated United States Geological Survey (USGS) data used in default WRF initial static field. The 17 MODIS land-use categories defined by the International Geosphere Biosphere Program (IGBP) were mapped onto the 24 USGS categories. Default CLM4 prescribes the sub-grid PFT composition for each land category in USGS, leading to geographical-invariant plant distribution. We represented the sub-grid surface heterogeneity in this study as the composition of 500 m-resolved land categories contained in a 12 km-resolved model grid. A total of 12 vegetation categories in IGBP were converted to 7 PFTs used in the CLM4 scheme. The conversion of IGBP land cover into USGS and PFTs was illustrated in Table S3. The spatial distribution of 7 PFTs was shown in Fig.S1 (the small islands in the South China Sea are not included).

LAI data used in the default CLM4 scheme are updated daily by linearly interpolating between prescribed monthly values. In this study, the MODIS LAI data derived from MCD15A2H version 6 with a spatial resolution of 500 m and temporal resolution of 8 days was introduced to CLM4. The seasonal and regional patterns of LAI were shown in Figure S2 (the small islands in the South China Sea are not included). The sub-grid PFT-specific LAI was averaged over the fraction of the land area covered by each PFT within the grid cell. The same LAI data was used as current LAI (LAIc) for 8 days and the past 8-day image was considered as LAI of the previous time step (LAIp). The changes between LAIc and LAIp was used to determine leaf age (Guenther et al., 2006).

2.3 Numerical experiments

The simulations with the WRF version 4 were performed on a domain at 12 km horizontal resolution covering China and its surrounding areas with 420 × 380 cells in the horizontal direction and 35 layers in the vertical direction, extending from the surface to 50 hPa. The initial meteorological fields and boundary conditions were from the 6 h NCEP (National Centers for Environmental Prediction) global final analysis with a 1° × 1° spatial resolution. The meteorological fields were initialized at the start of each model run, which covered one month to account for the effects of canopy climate history. We designed four scenarios to evaluate the influence of parameter applications as follows: (1) BASE: standard configuration; (2) C1_T2: replacing leaf temperature with the air temperature at 2 m height; (3) C2_FSUN: neglecting shaded leaves; (4) C3_FIX: using fixed values for variables related to weather history. The simulation time of the BASE case covered the entire year of 2018, while other cases were only performed for July.

3 Results and Discussions

3.1 Evaluation of WRF output

Since the temperature and solar radiation exert primary control on BVOC emissions, we evaluated the WRF model performance in simulating the air temperature at 2 m height (T2) and the downward shortwave radiation (SWDOWN). The meteorology observations from 362 sites and daily solar radiation observations from100 sites in China were used for comparison. The in-situ meteorology observations are provided by the National Climatic Data Center (NCDC, https://www.ncdc.noaa.gov/) and radiation observations are derived from the National Meteorological Information Center (https://data.cma.cn/). The statistical analyses for four seasons are displayed in Table 1. The mean error (ME), mean bias (MB), correlation coefficient (r), and root-mean-square error (RMSE) of hourly T2 series are 1.70, −0.52, 0.98, 2.51℃, respectively. The r value in summer (0.90) is relatively lower than those in spring (0.95), autumn (0.96), winter (0.97), and the simulation shows slight cooling bias in spring, autumn, and winter. The ME, MB, r, RMSE values of the SWDOWN are 71.01, 69.82, 0.86, and 71.11 W m^{-2}. The simulated SWDOWN was ~45% higher than measured data. Overestimated solar radiation is a common issue of WRF model which could be attributed to neglect of radiation effect of aerosols (Lu and Kueppers, 2012). The simulations of WRF-CLM4 successfully reproduced the temporal and spatial patterns of T2 and SWDOWN (Figure S2). Generally, comparisons with observed data indicate that WRF-CLM4 provide a good simulation on meteorological conditions that are desirable for driving the MEGAN algorithm.

Table 1 *Verification Statistics of Air Temperature at 2 m Height (T2) and Downward Shortwave Radiation (SWDOWN).*

Variable	Season	Mean Obs. [a]	Mean Sim. [a]	ME [b]	MB [b]	*r* [b]	RMSE [b]
T2 (°C)	Spring	13.99	13.95	1.54	−0.04	0.95	2.26
	Summer	23.60	23.65	1.64	0.05	0.90	2.54
	Autumn	12.70	12.10	1.47	−0.60	0.96	2.16
	Winter	−1.34	−2.84	2.17	−1.50	0.97	3.00
	Year	12.23	11.70	1.70	−0.52	0.98	2.51
SWDOWN ($W\ m^{-2}$)	Spring	176.39	261.75	85.98	85.37	0.64	90.40
	Summer	192.25	278.29	86.50	86.05	0.59	92.00
	Autumn	129.03	184.58	57.86	55.55	0.59	61.89
	Winter	92.04	144.36	53.69	52.32	0.71	57.60
	Year	147.43	217.25	71.01	69.82	0.86	77.11

[a] Obs.: Mean observed value, Sim.: Mean simulated value;
[b] ME: Mean Error, MB: Mean Bias, *r*: correlation coefficient, RMSE: Root Mean Square Error.

3.2 Impacts of physiological variables application on estimations

The primary advantage of the coupling of WRF-CLM4-MEGAN is that MEGAN is driven by real-time physiological variables derived from vegetation physics. Here we discussed how the physiological parameter application affects estimations.

3.2.1. Effects of considering the leaf-air temperature bias

The difference between vegetation and air temperature is PFT-dependent due to different physiological conditions. Figure 1 displays the daily profiles of average leaf-air temperature bias. Due to the weak BVOC emission capacities of grass and crop, as well as the limited biomass in most time of the year, the temperature of grass and crop was not discussed here. The daily variety indicated that plants were cooler than the ambient environment in the night and warmer in the daytime, with positive bias peaked at 12:00~13:00 LT (Local Time). However, the maximum bias varied significantly among PFTs and seasons. The maximum leaf-temperature bias of evergreen trees remains relatively low and stable over seasons, ranging from 0.5 K to 1.5 K for evergreen broadleaf trees and 2 K to 4 K for evergreen needleleaf trees. The temperature bias of deciduous trees and shrubs was similar to that of evergreen trees in summer, but the maximum bias in winter was higher than that in summer by 3~8 K. The greatest difference between winter and summer maximum bias was found in simulations of deciduous broadleaf trees.

Varieties in the maximum temperature bias and its seasonal pattern indicated a strong relation between leaf-air temperature bias and leaf biomass. In summer, strong transpiration of leaves cool the vegetation effectively and prevent the leaf temperature from rising rapidly under sunlight. The leaf biomass of evergreen trees did not change significantly over the year, so the temperature bias remains stable among seasons. The cooling effect of transpiration was extremely low in winter for deciduous plants. Therefore, the vegetation was significantly warmed by solar radiation absorbed by stems, resulting in a large positive bias between vegetation and air temperature.

Wei et al. (2012) measured the canopy temperature and micrometeorological data of *Quercus variabilis*, a typical broadleaf deciduous tree, during the growing season (May to August). They reported that the mean canopy temperature was 3.55 K higher than air temperature during the daytime. The simulated result of our study was 2.2 K. Song et al. (2017) found a positive bias within 2 K between canopy and air temperature for broadleaf evergreen trees in Xishuangbanna, southwestern China. The simulated leaf-air temperature bias of broadleaf evergreen trees in our study was ~1.5 K. These comparisons indicated the good model performance on simulating the leaf temperature of major BVOC sources.

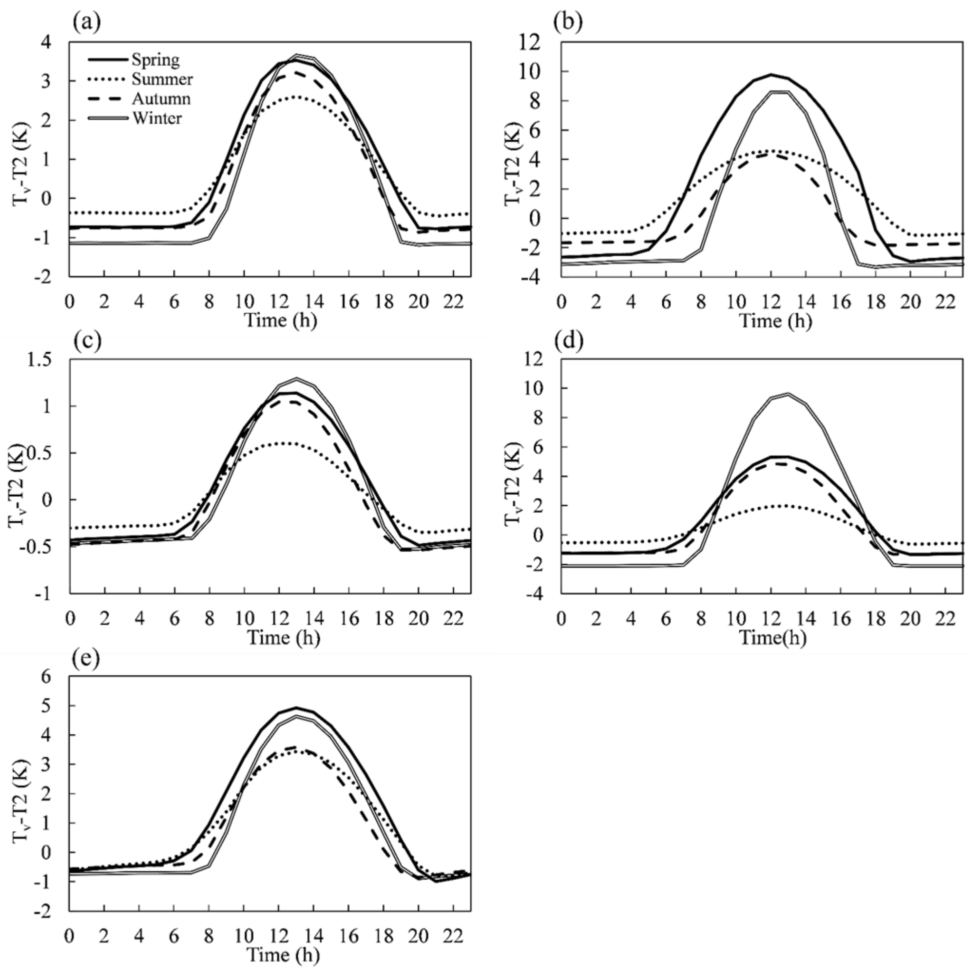

Figure 1 *Daily Profile of Differences in Average Leaf Temperature (T_v) and Air Temperature at 2 m Height (T2), (a) evergreen needleleaf trees, (b) deciduous needleleaf trees, (c) evergreen broadleaf trees, (d) deciduous broadleaf trees, (e) shrub.*

Many studies assumed that the leaf temperature was equal to air temperature in BVOC estimations. A model experiment used air temperature at 2 m height (C1_T2) for BVOC estimation was performed for July to investigate the impacts of considering leaf-air temperature bias on emissions. Emissions of isoprene and monoterpene from each PFT estimated in BASE and C1_T2 scenarios are listed in Table 2. Using T2 underestimated the total isoprene emission and monoterpene emission by 23.9% and 21.9%, respectively. The most significant underestimation was found in regions covered by shrub (underestimated by 58.6%). As a result of the small temperature bias in summer, isoprene and monoterpene emissions from broadleaf deciduous trees were only underestimated by 13.8% and 9.0% in C1_T2, respectively. However, due to the strong emission capacity, this underestimation contributed to 30% to the total emission difference. Therefore, due to variations in physiological parameters among tree species, the impact of unreasonable temperature applications varies greatly among PFTs. To reduce uncertainty, it is necessary to use PFT-specific leaf temperature for BVOC estimation.

3.2.2 Effects of differentiating between sunlit and shaded canopy

In CLM4 scheme, shaded leaves affect radiation distribution within the canopy by absorbing part of diffuse radiation. The sunlit/shaded fraction of the canopy was determined by leaf biomass and orientation, and the angle of the incident light. Variations in the sunlit fraction of each PFT (daytime in July) due to changes in solar zenith angle are shown in Fig. 2. For all PFTs, the fraction of sunlit canopy increased with increasing cosine of solar zenith angle, while the maximum fraction varied greatly. Due to the dense canopy in summer, trees have a smaller sunlit fraction than other PFTs under the same solar angle. The maximum fraction of trees was estimated to be 0.35. Because the leaf biomass in July of evergreen and deciduous trees was similar to each other, these trees showed a same trend in sunlit fraction with changes in solar angle. The radiation distribution among the sub-grid PFTs was considered in CLM4. When the light was coming in vertically, few radiations could be received by shrubs due to the absorption and reflection of higher canopies the same model grid. CLM4 assumes that the sunlit fraction is equal to 1 when the leaf area index exposed to light is lower than 0.01 m^2 m^{-2}. Therefore, the sunlit fraction of shrub was set as 1 under vertically incident light in this study. The largest sunlit fraction of grass and crop was 0.7 and 0.5, respectively.

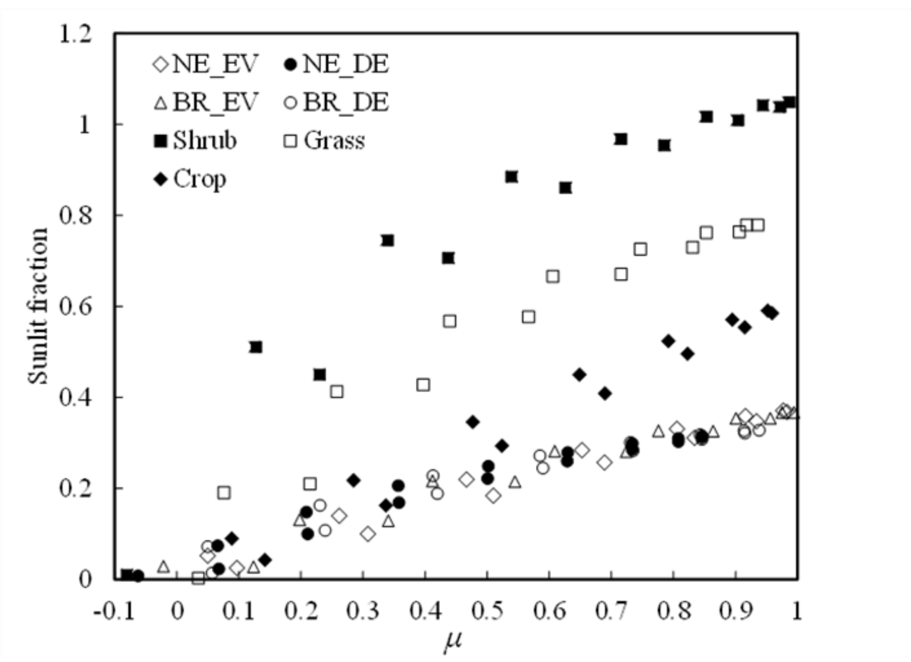

Figure 2 *Variations in sunlit fraction of each PFT under changing cosine of solar zenith angle (μ), The meaning of NE_EV, NE_DE, BR_EV and BR_DE refers to Table 2.*

Table 2 *Estimations of PFT-specific Isoprene and Monoterpene Emission in Each Scenario (Gg C).*

PFT	Scenario	Isoprene	Monoterpenes
NE_EV[a]	BASE	12.3	19.1
	C1_T2[b]	9.4	16.4
	C2_FSUN[b]	32.5	27.0
	C3_FIX[b]	6.3	17.3
NE_DE[a]	BASE	1.3	26.7
	C1_T2	0.9	20.2
	C2_FSUN	2.7	35.7
	C3_FIX	0.8	21.3
BR_EV[a]	BASE	249.6	56.4
	C1_T2	235.8	55.4
	C2_FSUN	663.2	83.4
	C3_FIX	121.3	48.1
BR_DE[a]	BASE	1404.0	409.6
	C1_T2	1210.0	372.6
	C2_FSUN	3764.0	623.2
	C3_FIX	681.3	341.1
Shrub	BASE	506.2	170.6
	C1_T2	209.5	69.1
	C2_FSUN	1166.0	243.2
	C3_FIX	180.3	134.4
Grass	BASE	57.2	2.6
	C1_T2	31.9	1.4
	C2_FSUN	95.3	3.4
	C3_FIX	22.5	1.6
Crop	BASE	35.6	12.3
	C1_T2	27.1	8.9
	C2_FSUN	79.1	18.6
	C3_FIX	12.6	9.1
Total	BASE	2266.1	697.2
	C1_T2	1724.5	544.2
	C2_FSUN	5802.8	1034.4
	C3_FIX	1025.5	572.9

[a]NE_EV: Needleleaf Evergreen Tree; NE_DE: Needleleaf Deciduous Tree; BR_EV: Broadleaf evergreen Tree; BR_DE: Broadleaf Deciduous Tree;
[b]C1_T2: replacing leaf temperature with air temperature at 2 m to parameterize temperature response; C2_FSUN: ignoring the fractions of sunlit and shaded leaves; C3_FIX: using fixed values for variables that related to weather history.

Since the simplified BVOC algorithms were not able to separate the canopy, previous studies assumed that all the radiation was received by sunlit leaves. Figure 3 displays the difference in solar radiation absorbed by the sunlit canopy (daytime in July) in differentiating between sunlit and shaded canopy or not (excluding small islands in the South China Sea). Because the shadowed canopy absorbed a part of diffuse solar radiation, taking shadowed canopy into account resulted in a decrease in total radiation absorbed by sunlit leaves. While the radiation absorbed by shrub and grass showed little difference between the two cases, radiation absorbed by trees was generally overestimated by over 50% in the scenario which neglected shaded leaves.

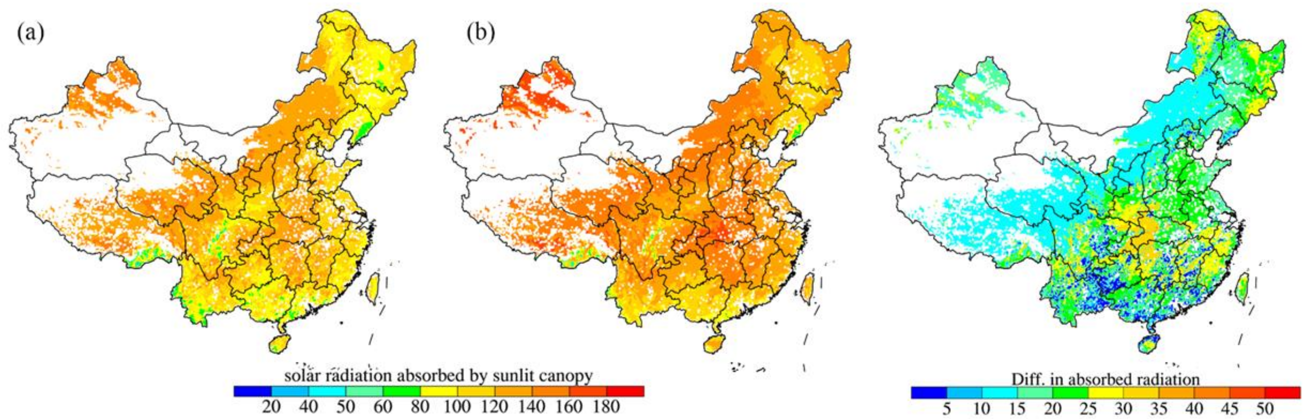

Figure 3 *Difference in solar radiation absorbed by sunlit canopy during daytime in July between cases considering or not considering sunlit/shaded leaves separately. (a) separate treatments of canopy; (b) no separate treatments.*

Leaf-level radiation controls estimation of radiation response of BVOC emission rates. To investigate the effects of differentiating between sunlit and shaded canopy, the fraction of shaded leaves was neglected in the C2_FSUN scenario. The results of C2_FSUN are listed in Table 2. C2_FSUN overestimated isoprene and monoterpene emissions in July by a factor of 2.6 and 1.5, respectively. Emissions from broadleaf and needleleaf trees were overestimated by a factor of 2.7 due to the large fractions of shadowed leaves in summer. The least discrepancy was found in the estimation of grass emissions, which were within a factor of 2 of the BASE estimations. In conclusion, ignoring the shaded part of the canopy could significantly overestimate BVOC emissions.

3.2.3 Effects of improved parameterization of medium-term weather history

MEGAN algorithms require average leaf temperature and solar radiation over past days to simulate the emission response to medium-term environmental changes. In the original WRF-CLM4 scheme, the accumulated module used to calculate running mean leaf temperature and leaf fraction was inactive. Variables based on weather history were assigned with fixed values. In this study, we modified this module to provide dynamic past-day's physiological parameters for the MEGAN algorithm. We conducted C3_FIX scenario to investigate the impacts (Table 2). Emission of isoprene and monoterpene in C3_FIX was lower than that estimated in BASE by 54.7% and 17.8%, respectively. The relatively slight influence on monoterpene emissions could be attributed to the partial dependence of monoterpene emissions on solar radiation. Isoprene emission is highly sensitive to solar radiation so that variations in past-time's leaf fraction and PAR greatly affected isoprene emission estimation. Emissions from needleleaf trees were underestimated by about 40% and those from other PFTs were underestimated by about 60%. We further calculated emissions in January using fixed values (not shown). The isoprene and monoterpene emissions were estimated as 64.7 (61.3 in BASE) and 36.4 Gg C (34.0 in BASE), respectively. The discrepancy between using fixed and dynamic values was within 10%. Although the fixed values could make estimations similar to dynamic variables in low temperature and radiation conditions, using fixed values for all seasons leads to significant uncertainty.

3.3 BVOC emission budgets and spatiotemporal distribution

Hourly emissions of 8 chemical species were calculated by the WRF-CLM4-MEGAN model on a 12 km×12 km grid for the year 2018. In the following section, all the results are measured as carbon weights of the constituent compounds, unless stated otherwise.

The annual amount emitted for all listed BVOCs reaches 14.7 Tg C with isoprene accounting for 78.3% (11.5 Tg) and the sum of monoterpenes for 21.7% (3.2 Tg). Emissions from each PFT are shown in Table 3. Province-level emissions are listed in Table S4. For both isoprene and monoterpene, the predominant source was broadleaf deciduous forests with a contribution of 64.5% and 60.6% to isoprene and monoterpene, respectively. Shrubs ranked second of the emission contribution, accounting for 19.9% of total BVOC emissions, followed by broadleaf evergreen trees (12.1%). Grass and Crop were responsible for only 1.3% of total isoprene emission and 1.1% of monoterpene emission.

Table 3 *BVOC Emission Budgets of Each Plant Functional Type (PFT) (Gg C).*

PFTs	ISO [b]	MT [a]								T_ALL [c]
		API [b]	BPI [b]	3-CAR[b]	OCI [b]	LIM [b]	SAB [b]	MYR [b]	T_MT [c]	
NE_EV [a]	59.3	35.6	38.6	20.6	3.4	12.9	5.0	5.0	121.0	180.3
NE_DE [a]	4.2	33.7	20.0	8.0	3.0	13.0	2.6	4.0	84.4	88.6
BR_EV [a]	1421.0	169.0	61.6	20.5	28.8	41.0	22.5	22.5	365.8	1786.8
BR_DE [a]	7442.0	806.6	426.0	97.8	179.7	262.4	100.8	60.2	1934.0	9376.0
Shrub	2295.0	183.3	132.7	89.0	70.9	89.0	42.9	30.6	638.3	2933.3
Grass	188.1	2.2	2.2	0.3	1.8	1.0	0.7	0.2	8.4	196.5
Crop	119.4	9.2	9.9	2.0	7.4	4.6	3.2	1.4	37.8	157.2
Nation	11528	1240	691	242	295	424	178	124	3193	14721

[a]Refer to Table 2;
[b]ISO: isoprene, API: α-pinene, BPI: β-pinene, 3-CAR: 3-carene, OCI: ocimene, LIM: limonene, SAB: sabinene, MYR: myrcene;
[c]T_MT: Total monoterpenes emissions of each PFT, T_ALL: Total BVOC (includes isoprene and monoterpenes) emissions of each PFT.

The spatial distributions of annual emissions of isoprene and monoterpenes are displayed in Fig.4 (excluding small islands in the South China Sea). The south and northeast of China, as well as the Qinling Mountains in central China, were estimated with high emission budgets, accounting for 91.3% of the national isoprene emission and 91.8% of the monoterpene emission. According to Fig.S1 and the survey results from the Plant Research Institute, these areas are covered by vegetation species with a high emission capacity of isoprene (broadleaf forests, shrub) or monoterpenes (coniferous forest). Northeast China is primarily covered by deciduous coniferous forests (mainly *Larix gmelini*) and deciduous broadleaf forests (mainly *Quercus mongolica*, *Tilia Mongolia*, and *Betula platyphylla*). Large areas of evergreen coniferous forests (mainly *Pinus massoniana* and *Cunninghamia lanceolata*) and shrubs are found in Southeast China, and the main plant genera in Southwest China are evergreen tree species, including evergreen broadleaf forests (e.g. *Quercus aquifolioides*), evergreen coniferous forests (*Picea likiangensis var.balfouriana* and *Pinus yunnanensis*) and shrubs. The Qinling Mountains are covered by large areas of deciduous broadleaf forests (mainly *Quercus variabilis* and *Quercus liaotungensis*). Regions covered by a large area of crop or grassland, such as the North China Plain and Inner Mongolia, played a very small role in BVOC budgets due to the low emitting capacities.

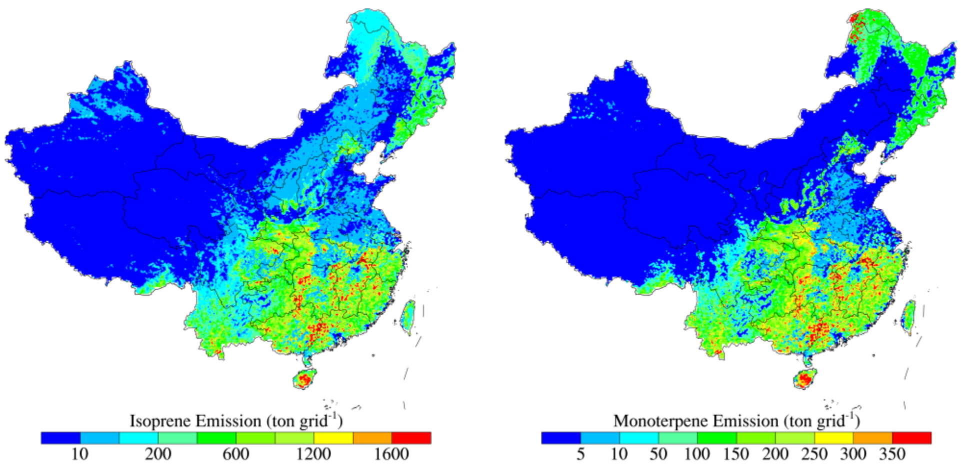

Figure 4 *Spatial distribution of isoprene and monoterpenes emissions in the year 2018.*

BVOC emissions showed strong seasonal variation. The temporal profile of national monthly emissions of individual species is presented in Fig.5. Because of the highest light intensities, temperatures, and plant biomass density, the emissions peaked in summer (from June to August) and around 55.1% (8.1 Tg C) of the total annual budgets were released during this period. Previous studies estimated the highest emissions in July; however, our results showed a higher emission in August. This could be attributed to the consideration of the effects of canopy climate history on estimation. This results were consistent with a whole-year measurement reported by Chen et al. (2020).

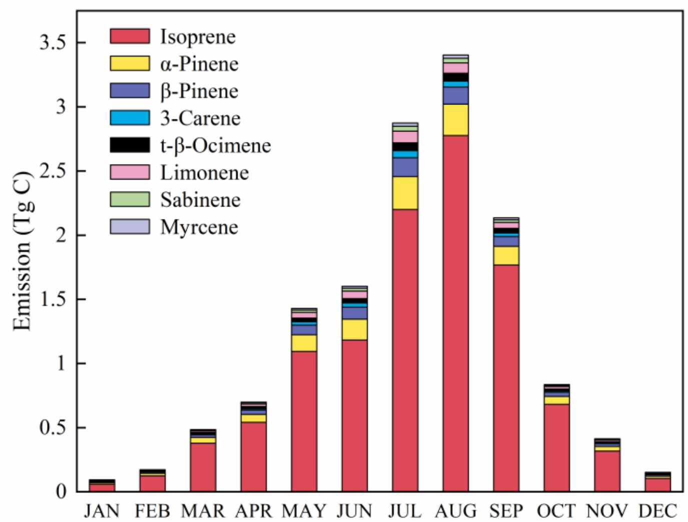

Figure 5 *Monthly variations in BVOC emission budget (Tg C).*

The diurnal variations of temperature, solar radiation, and emission of isoprene and monoterpenes in summer are shown in Fig.6. Simulated emissions increased rapidly in the morning and peaked in the afternoon. Time for peak emissions was closed to time for the highest leaf temperature and solar radiation, while T2 reached the highest value about an hour later. Emissions of monoterpenes are not highly dependent on the light while isoprene emissions are strong light-dependent. As a result, monoterpene emissions maintain a relatively high level during the night while isoprene emissions cease at nighttime.

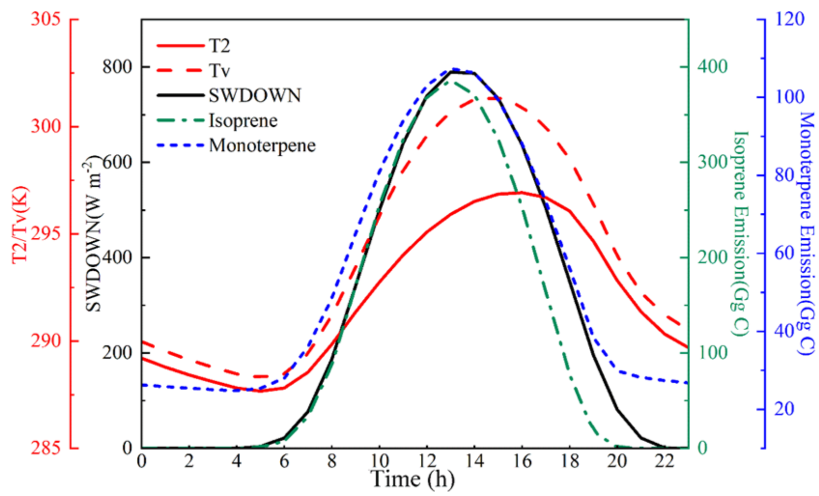

Figure 6 *Diurnal variations in summer of air temperature at 2 m height (T2), leaf temperature (Tv), downward solar radiation (SWDOWN) and emissions of isoprene and monoterpenes (Gg C).*

3.4 Comparisons with previous studies

We evaluated the inventory against canopy-scale measurements conducted at different sites in China. Given that years of interest in the present study and observations are different, the average data or monthly total emissions were used for comparison.

Using the eddy covariance technique, Baker et al. (2005) measured isoprene fluxes in Xishuangbanna, Yunnan Province (21.92°N, 101.27°E). Daytime isoprene fluxes during the wet season (July 2002) was approximately 1 mg C m^{-2} h^{-1}. Our model predicted the daytime average isoprene flux over July as 1.5 mg C m^{-2} h^{-1}, similar to the observed data. Based on Relaxed Eddy Accumulation (REA) technique, emissions of isoprene and monoterpenes of a temperate forest in Changbai Mountain (42.4°N, 128.1°E) were measured during the summer seasons in 2010 and 2011 (Bai et al., 2015). Average isoprene fluxes were measured as 1.3 and 1.5 mg m^{-2} h^{-1}, and the simulated fluxes were 2.1 and 2.0 mg m^{-2} h^{-1}, respectively, about 50% higher than observations. The average PAR and temperature during experimental periods were 837.5 μmol m^{-2} s^{-1} and 22.6 ℃, respectively. The simulation resulted in an average PAR of 1160.1 μmol m^{-2} s^{-1} and a temperature of 22.23 ℃. The average leaf temperature was 23.37 ℃. The slight overestimation could be attributed to higher PAR in the model.

Using REA method, Bai et al. (2016) measured emissions from a bamboo (*Phyllostachys violascenes*) plantation in Zhejiang Province (30.3°N, 119.57°E) and the average isoprene emission fluxes were 2.81, 1.07, 0.186, 0.068 mg m^{-2} h^{-1} for the experimental periods in July, August, September, and October. The predicted monthly average fluxes were 2.04, 1.95, 0.39, 0.14 mg m^{-2} h^{-1}, respectively. Estimations were within a factor of 2 of observed values.

As illustrated in Table 4, the annual emission budgets estimated by this study fall in the range of past studies. Both the improvement in driving variables and the representation of sub-grid plant composition contribute to the difference in estimates. Formaldehyde (HCHO), as a major intermediate product in the degradation of isoprene in the atmosphere, has been widely used as a proxy for estimates isoprene emissions. Fu et al. (2007) used a continuous 6-year record (1996–2001) of Global Ozone Monitoring Experiment (GOME) HCHO columns to estimate isoprene emission as 12.7 Tg yr^{-1} in China, which is comparable to our model outputs. Stavrakou et al. (2014) found that isoprene emissions in China decrease from 8.6 Tg in the year 2007 to 6.5 Tg in the year 2012 based on GOME-2 HCHO columns, lower than emissions in this study by 33.7%~76.9%. The isoprene emission from China in 2010 was estimated to be 6.5 Tg based on OMI (Ozone Monitoring Instrument) HCHO observations (Stavrakou et al., 2015). Aside from the influence of different meteorological conditions and land cover changes during the past years, the reliability of satellite-based constraints also needs to be improved (Fu et al., 2019).

Table 4 *Comparison of BVOC Budgets (Tg C yr^{-1}) estimated in This Study and in Previous Studies.*

Base year	Emission Budget			Reference
	ISO [a]	MT [a]	Total	
2018	11.5	3.2	14.7	This study
-	15.0	4.3	19.3	Guenther et al. (1995) [a]
-	4.1	3.5	7.6	Klinger et al. (2002) [a]
2004	6.8	2.8	9.6	Tie et al. (2006) [b]
2000	10.0	2.5	12.5	Guenther et al. (2006) [c]
Averaged over 2001-2006	9.6	2.8	12.4	Fu and Liao (2012) [c]
-	12.7			Fu et al. (2007) [d]
2010	5.9			Stavrakou et al. (2014) [d]
2010	6.5			Stavrakou et al. (2015) [e]

[a]Based on G95 algorithms (Guenther et al., 1995);
[b]Based on G20 algorithms (Guenther et al., 2000);
[c]Based on MEGAN2.0 algorithms (Guenther et al., 2006);
[d]Top-down annual emission estimates which were inferred by inversion of GOME-2 formaldehyde columns.
[e]Top-down annual emission estimates which were inferred by inversion of OMI formaldehyde columns

4 Uncertainty

The basal emission factors are identified as the most important uncertainty source in BVOC emission estimations (Guenther et al., 2006). Local emission factors for isoprene reported by previous observations conducted in China were used in this study. Since measurements of the monoterpene emission factors are scarce, we calculated local emission factors based on the ratio of local isoprene emission factor to default emission factor in MEGAN literature. There are large uncertainties associated with the conversion approach. More in-situ observations on emission rates of different PFTs in China are required.

CLM4 parameterizes one layer of the canopy, however, solar radiation is attenuated by foliage and leaf temperature varies among layers. A relatively simple representation of canopy is also a source of uncertainty. Guenther et al. (1995) found a less than 5% difference in global annual isoprene emission estimated with one or five lays and no change in the estimations of other BVOC emissions, suggesting that BVOC emissions are relatively insensitive to the number layers. However, many studies indicated that the treatment of microclimatic factors such as light and leaf temperature within the canopy resulted in a substantial difference in estimated emissions (Keenan et al., 2011).

5 Conclusions

This study estimated the emission budgets and spatial-temporal patterns of BVOC in China in the year 2018 using the WRF-CLM4-MEGAN modeling system. This framework improved biogenic emission estimations by using PFT-specific physiological parameters derived from soil and vegetation physics in the CLM4 scheme. The simulated vegetation temperature was typically higher than air temperature by 1~12 K in the daytime and lower than ambient value by approximately 2 K during the night. Using air temperature instead of leaf temperature underestimated isoprene and monoterpene emissions in July by 23.9% and 21.9%, respectively. Because the shaded fraction of broadleaf trees could be higher than 60 % in July, ignoring the influence of shaded canopy on radiation distribution overestimated emissions by a factor of 2.6. Assigning fixed values to variables that related to weather history made a similar estimation to that based on dynamic variables in January, while underestimated emissions in July by approximately 50%. Due to the significant discrepancy caused by these physiological variables, more reasonable parameter applications are important for accurately estimating biogenic emissions. Using the CLM4-MEGAN framework, the annual emissions of BVOC in China was estimated to be 14.7 Tg C, with isoprene and monoterpenes accounting for 78.3% and 21.7% of the totals, respectively. The coupled model successfully reproduced the spatial and temporal patterns of BVOC emissions. The predicted values were within a factor of 2 of most observed values. Comparisons indicated that this coupled model are able to estimate BVOC emissions reasonably in China.

Acknowledgments and **Data**

The MODIS land cover data (MCD12Q1), water mask data (MOD44W) and leaf are index product (MCD15A2H) were provided by Land Process Distributed Active Archive Center (LPDAAC), USA.

The MCD12Q1 product can be freely accessed at 10.5067/MODIS/MCD12Q1.006. MOD44W data can be download from 10.5067/MODIS/MOD44W.006. MCD15A2H data can be found at 10.5067/MODIS/MCD15A2H.006.

This work was supported by the National Natural Science Foundation of China (NSFC) (41675142, 91644212).

This work was designed by YS, XC, LK and HZ, and performed by LY, ZX, ML, TX, TW, WL and ML. LY and YS led the writing of the papers and prepared the figures with contributions from all co-authors.

The authors declare that they have no conflict of interest.

References

Arneth, A., P. A. Miller, M. Scholze, T. Hickler, G. Schurgers, B. Smith, and I. C. Prentice (2007), CO2 inhibition of global terrestrial isoprene emissions: Potential implications for atmospheric chemistry, *Geophysical Research Letters*, *34*(18), doi:10.1029/2007gl030615.

Bai, J., A. Guenther, A. Turnipseed, and T. Duhl (2015), Seasonal and interannual variations in whole-ecosystem isoprene and monoterpene emissions from a temperate mixed forest in Northern China, *Atmospheric Pollution Research*, *6*(4), 696-707, doi:10.5094/APR.2015.078.

Bai, J., A. Guenther, A. Turnipseed, T. Duhl, S. Yu, and B. Wang (2016), Seasonal variations in whole-ecosystem BVOC emissions from a subtropical bamboo plantation in China, *Atmospheric Environment*, *124*, 12-21, doi:10.1016/j.atmosenv.2015.11.008.

Baker, B., et al. (2005), Wet and dry season ecosystem level fluxes of isoprene and monoterpenes from a southeast Asian secondary forest and rubber tree plantation, *Atmospheric Environment*, *39*(2), 381-390, doi:10.1016/j.atmosenv.2004.07.033.

Chen, C., et al. (2019), China and India lead in greening of the world through land-use management, *Nature Sustainability*, *2*(2), 122-129, doi:10.1038/s41893-019-0220-7.

Chen, J., J. Tang, and X. Yu (2020), Environmental and physiological controls on diurnal and seasonal patterns of biogenic volatile organic compound emissions from five dominant woody species under field conditions, *Environmental Pollution*, *259*, 113955, doi:10.1016/j.envpol.2020.113955.

Fehsenfeld, F., et al. (1992), Emissions of volatile organic compounds from vegetation and the implications for atmospheric chemistry, *Global Biogeochemical Cycles*, *6*(4), 389-430, doi:10.1029/92gb02125.

Fu, D., D. B. Millet, K. C. Wells, V. H. Payne, S. Yu, A. Guenther, and A. Eldering (2019), Direct retrieval of isoprene from satellite-based infrared measurements, *Nature Communications*, *10*(1), 3811, doi:10.1038/s41467-019-11835-0.

Fu, T.-M., D. J. Jacob, P. I. Palmer, K. Chance, Y. X. Wang, B. Barletta, D. R. Blake, J. C. Stanton, and M. J. Pilling (2007), Space-based formaldehyde measurements as constraints on volatile organic compound emissions in east and south Asia and implications for ozone, *Journal of Geophysical Research: Atmospheres*, *112*(D6), doi:10.1029/2006jd007853.

Fu, Y., and H. Liao (2012), Simulation of the interannual variations of biogenic emissions of volatile organic compounds in China: Impacts on tropospheric ozone and secondary organic aerosol, *Atmospheric Environment*, *59*, 170-185, doi:10.1016/j.atmosenv.2012.05.053.

Guenther, A., C. N. Hewitt, D. Erickson, R. Fall, C. Geron, T. Graedel, P. Harley, L. Klinger, M. Lerdau, and W. McKay (1995), A global model of natural volatile organic compound emissions, *Journal of Geophysical Research: Atmospheres*, *100*(D5), 8873-8892.

Guenther, A., T. Karl, P. Harley, C. Wiedinmyer, P. I. Palmer, and C. Geron (2006), Estimates of global terrestrial isoprene emissions using MEGAN (Model of Emissions of Gases and Aerosols from Nature), *Atmos. Chem. Phys.*, *6*(11), 3181-3210, doi:10.5194/acp-6-3181-2006.

Guenther, A. B., X. Jiang, C. L. Heald, T. Sakulyanontvittaya, T. Duhl, L. K. Emmons, and X. Wang (2012), The Model of Emissions of Gases and Aerosols from Nature version 2.1 (MEGAN2.1): an extended and updated framework for modeling biogenic emissions, *Geosci. Model Dev.*, *5*(6), 1471-1492, doi:10.5194/gmd-5-1471-2012.

Guenther, A. B., R. K. Monson, and R. Fall (1991), Isoprene and monoterpene emission rate variability: Observations with eucalyptus and emission rate algorithm development, *Journal of Geophysical Research: Atmospheres*, *96*(D6), 10799-10808, doi:10.1029/91jd00960.

Henrot, A. J., T. Stanelle, S. Schröder, C. Siegenthaler, D. Taraborrelli, and M. G. Schultz (2017), Implementation of the MEGAN (v2.1) biogenic emission model in the ECHAM6-HAMMOZ chemistry climate model, *Geosci. Model Dev.*, *10*(2), 903-926, doi:10.5194/gmd-10-903-2017.

Jin, J., N. L. Miller, and N. Schlegel (2010), Sensitivity Study of Four Land Surface Schemes in the WRF Model, *Advances in Meteorology*, *2010*, 11, doi:10.1155/2010/167436.

Jin, J., and L. Wen (2012), Evaluation of snowmelt simulation in the Weather Research and Forecasting model, *Journal of Geophysical Research: Atmospheres*, *117*(D10), doi:10.1029/2011jd016980.

Keenan, T. F., R. Grote, and S. Sabaté (2011), Overlooking the canopy: The importance of canopy structure in scaling isoprenoid emissions from the leaf to the landscape, *Ecological Modelling*, *222*(3), 737-747, doi:10.1016/j.ecolmodel.2010.11.004.

Klinger, L. F., Q.-J. Li, A. B. Guenther, J. P. Greenberg, B. Baker, and J.-H. Bai (2002), Assessment of volatile organic compound emissions from ecosystems of China, *Journal of Geophysical Research: Atmospheres*, *107*(D21), ACH 16-11-ACH 16-21, doi:10.1029/2001jd001076.

Lawrence, D. M., et al. (2011), Parameterization Improvements and Functional and Structural Advances in Version 4 of the Community Land Model, *Journal of Advances in Modeling Earth Systems*, *3*, doi:10.1029/2011ms000045.

Levis, S., C. Wiedinmyer, G. B. Bonan, and A. Guenther (2003), Simulating biogenic volatile organic compound emissions in the Community Climate System Model, *Journal of Geophysical Research: Atmospheres*, *108*(D21), doi:10.1029/2002jd003203.

Li, L. Y., Y. Chen, and S. D. Xie (2013), Spatio-temporal variation of biogenic volatile organic compounds emissions in China, *Environmental Pollution*, *182*, 157-168, doi:10.1016/j.envpol.2013.06.042.

Li, M., X. Huang, J. Li, and Y. Song (2012), Estimation of biogenic volatile organic compound (BVOC) emissions from the terrestrial ecosystem in China using real-time remote sensing data, *Atmos. Chem. Phys. Discuss.*, *2012*, 6551-6592, doi:10.5194/acpd-12-6551-2012.

Liu, Y., L. Li, J. Y. An, W. Zhang, R. S. Yan, L. Huang, C. Huang, H. L. Wang, Q. Wang, and M. Wang (2018), Emissions, Chemical Composition, and Spatial and Temporal Allocation of the BVOCs in the Yangtze River Delta Region in 2014.

Lu, Y., and L. M. Kueppers (2012), Surface energy partitioning over four dominant vegetation types across the United States in a coupled regional climate model (Weather Research and Forecasting Model 3–Community Land Model 3.5), *Journal of Geophysical Research: Atmospheres*, *117*(D6), doi:10.1029/2011jd016991.

Niinemets, Ü., G. Seufert, R. Steinbrecher, and J. D. Tenhunen (2002), A model coupling foliar monoterpene emissions to leaf photosynthetic characteristics in Mediterranean evergreen Quercus species, *New Phytologist*, *153*(2), 257-275, doi:10.1046/j.0028-646X.2001.00324.x.

Niinemets, Ü., J. D. Tenhunen, P. C. Harley, and R. Steinbrecher (1999), A model of isoprene emission based on energetic requirements for isoprene synthesis and leaf photosynthetic properties for Liquidambar and Quercus, *Plant, Cell & Environment*, *22*(11), 1319-1335, doi:10.1046/j.1365-3040.1999.00505.x.

Oleson, K., et al. (2010), *Technical Description of version 4.0 of the Community Land Model (CLM)*.

Sakulyanontvittaya, T., T. Duhl, C. Wiedinmyer, D. Helmig, S. Matsunaga, M. Potosnak, J. Milford, and A. Guenther (2008), Monoterpene and Sesquiterpene Emission Estimates for the United States, *Environmental Science & Technology*, *42*(5), 1623-1629, doi:10.1021/es702274e.

Schultz, N. M., X. Lee, P. J. Lawrence, D. M. Lawrence, and L. Zhao (2016), Assessing the use of subgrid land model output to study impacts of land cover change, *Journal of Geophysical Research: Atmospheres*, *121*(11), 6133-6147, doi:10.1002/2016jd025094.

Song, Q.-H., et al. (2017), Canopy temperature variability in a tropical rainforest, subtropical evergreen forest, and savanna forest in Southwest China, *iForest - Biogeosciences and Forestry*, *10*(3), 611-617, doi:10.3832/ifor2223-010.

Stavrakou, T., et al. (2015), How consistent are top-down hydrocarbon emissions based on formaldehyde observations from GOME-2 and OMI?, *Atmos. Chem. Phys.*, *15*(20), 11861-11884, doi:10.5194/acp-15-11861-2015.

Stavrakou, T., J. F. Müller, M. Bauwens, I. De Smedt, M. Van Roozendael, A. Guenther, M. Wild, and X. Xia (2014), Isoprene emissions over Asia 1979–2012: impact of climate and land-use changes, *Atmos. Chem. Phys.*, *14*(9), 4587-4605, doi:10.5194/acp-14-4587-2014.

Subin, Z. M., W. J. Riley, J. Jin, D. S. Christianson, M. S. Torn, and L. M. Kueppers (2011), Ecosystem Feedbacks to Climate Change in California: Development, Testing, and Analysis Using a Coupled Regional Atmosphere and Land Surface Model (WRF3-CLM3.5), *Earth Interactions*, *15*, doi:10.1175/2010ei331.1.

Tie, X., G. Li, Z. Ying, A. Guenther, and S. Madronich (2006), Biogenic emissions of isoprenoids and NO in China and comparison to anthropogenic emissions, *Science of The Total Environment*, *371*(1), 238-251, doi:10.1016/j.scitotenv.2006.06.025.

Wei, D. D., J. S. Zhang, M. Ping, Z. Ning, and Y. F. Ren (2012), Variations of canopy temperature in Quercus variabilis plantation and their relations with micrometeorological factors, *Chinese Journal of Applied Ecology*, *23*(7), 1767-1773.

Wu, K., et al. (2020), Estimation of biogenic VOC emissions and their corresponding impact on ozone and secondary organic aerosol formation in China, *Atmospheric Research*, *231*, 104656, doi:10.1016/j.atmosres.2019.104656.

Zhao, C., et al. (2016), Sensitivity of biogenic volatile organic compounds to land surface parameterizations and vegetation distributions in California, *Geosci. Model Dev.*, *9*(5), 1959-1976, doi:10.5194/gmd-9-1959-2016.